ENC 2012
EUROPEAN NUCLEAR CONFERENCE

Transactions
Simulations & GEN III

EUROPEAN NUCLEAR SOCIETY

ENS CONFERENCE

ENC 2012 Diamond Sponsor:

HITACHI

ENC 2012 Gold Sponsors:

AGORIA
no future without technology

Belgoprocess

SCK·CEN
STUDIECENTRUM VOOR KERNENERGIE
CENTRE D'ETUDE DE L'ENERGIE NUCLEAIRE

NUCLEAIR FORUM NUCLEAIRE

ENC 2012 Silver Sponsor:

urenco

ENC 2012 Sponsor:

ONET TECHNOLOGIES

organised in collaboration with:

the Nuclear Institute

IAEA International Atomic Energy Agency

NEA Nuclear Energy Agency

European Nuclear Society
Rue Belliard 65
1040 Brussels, Belgium
Phone + 32 2 505 30 54
Fax +32 2 502 39 02
E-mail ens@euronuclear.org
Internet www.euronuclear.org

ISBN 978-92-95064-14-0

These transactions contain all contributions submitted by 7 December 2012.

SIMULATIONS & GEN III

In Vessel Retention Analisys with Astec code

MIRCO DI GIULI, MARCO SUMINI, FABIANA ROSSI

Nuclear Engineering Laboratory, Dept. DIENCA University of Bologna

Via dei Colli, 16, 40136 Bologna, Italy

FELICE DE ROSA

ENEA, UTFISSM-SICSIS Via Martiri di Monte Sole,4, 40129 Bologna, Italy

ABSTRACT

A Severe Accident countermeasure can be the retention of the melted core inside the reactor vessel. A way to achieve this kind of corium retention is by removing heat from the steel vessel by flooding the reactor cavity. A first calculation was performed in order to assess In-Vessel Core Damage Retention (IVR) possibilities for an AP1000 reactor as a consequence of a Beyond Design Basis Accident (BDBA). The computer code used to perform this calculation is ASTEC. ASTEC is an integral code to analyse severe accidents in LWRs, jointly developed by IRSN (France) and GRS (Germany), and it is meant to predict a whole severe accident sequence from the initiating event to source term evaluation inside the containment building. The accidental transient was carried out using ICARE and CESAR modules for the evaluation of the primary system thermal-hydraulic behaviour. The improved debris bed and magma models available in the code last version have been used to describe the late phase of core degradation. In this calculation different assumptions were done regarding the corium, particularly different configurations of the corium relocated in the RPV lower head were considered. The results of the calculations show the effectiveness of the reactor cavity flooding option as a severe accident management strategy.

1. Introduction

The aim of this paper is to evaluate the effectiveness of the In Vessel Retention (IVR) severe accident management strategy, adopted by advanced light water reactors as AP1000, by means of the ASTEC code. ASTEC (Accident Source Term Evaluation Code) is an integral source term code developed by IRSN-GRS which has become the reference European code for the study of severe accidents (SAs) and reactor safety in generation II&III PWR [1]. Considering (SAs) represents an essential aspect of defense in depth concept used in nuclear safety of NPPs. SAs are accident conditions more severe than Design Basic Accidents (DBAs), which have very low probabilities of happening and could have significant consequences resulting from nuclear fuel degradation. Many phenomena as fuel failure, FPs transport in Primary Heat Transport system and containment system, core melting, corium formation and relocation, core-concrete interaction, etc. ask for a deep knowledge and understanding. The first part of this paper deals with an overview of the ASTEC code modeling used for the description of the AP1000. The second part proposes a summary of the scenario used to simulate the accident sequence. The third part summarizes the code results. The conclusion will be focused on the preliminary synthesis of the Severe Accident Code capabilities to simulate the IVR during the course of severe accident transient.

2. AP 1000 ASTEC MODELING

The nuclear steam supply system (NSSS) has the function to carry the hot water from the reactor vessel to the steam generators, where the steam is produced for driving the turbine, while maintaining constant all the parameters in the reactor. The NSSS model representing the AP1000 using ASTEC is illustrated in Figure 1. The operating conditions correspond to power uprate (PU), that is, the power rate is 3415 MWt. This model includes the following main elements, (1) reactor vessel and internals, (2) the reactor core, (3) the lower head of the reactor vessel, (4) steam generators, (5) main steam lines, (6) feed-water system. The control system and safety system are not illustrated in figure. The model of the vessel lower head is a fundamental element for the analysis in accident scenarios, seeing that the IVR interacts principally with this part of the vessel. Three ASTEC code module have been used to model the AP1000 reactor: CESAR module to describe the primary circuit, the secondary circuit, the control and safety systems; ICARE to model the core; RUPUICUV to model the cavity containing the reactor vessel. A detailed nodalisation has been used to describe the primary and secondary circuit: the first one has been subdivided in 61 volumes, the second one in 35 volumes [2]. The control and safety systems (pumps, pressurizer, valves etc) characteristics respect the original technical characteristics [3] [4]. The core has been discretised in 6 cylindrical rings and 21 axial meshes, only one representative component of the fuel and control rods being considered in each ring, weighted by the true number of rods . The different control systems taken into account are: pressurizer heaters, pressurizer spray ring, pressurizer relief valves, feed-water pumps, feed and bleed system, main steam line valves. Regarding safety systems have been considered the Reactor safety system, reactor makeup tanks, accumulators, auxiliary feed-water systems, isolation turbine system, steam dump valve. Different sensors to activate the control and safety systems are taken into account. All these systems have been considered in order to have a more correct simulation of the accident sequence in AP1000 reactor.

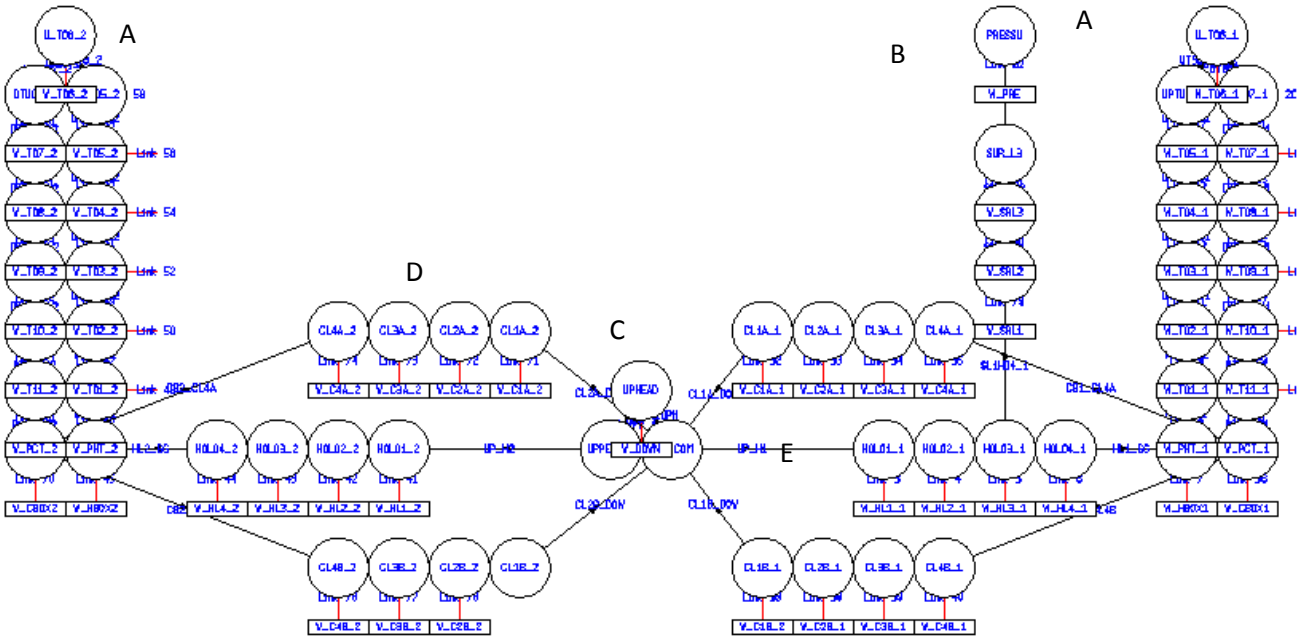

Fig.1 *Primary circuit nodalisation: A – U- tubes (SGs), B – Pressurizer, C – Upper head, Downcomer, Upper plenum, D – Cold leg, E – Hot leg*

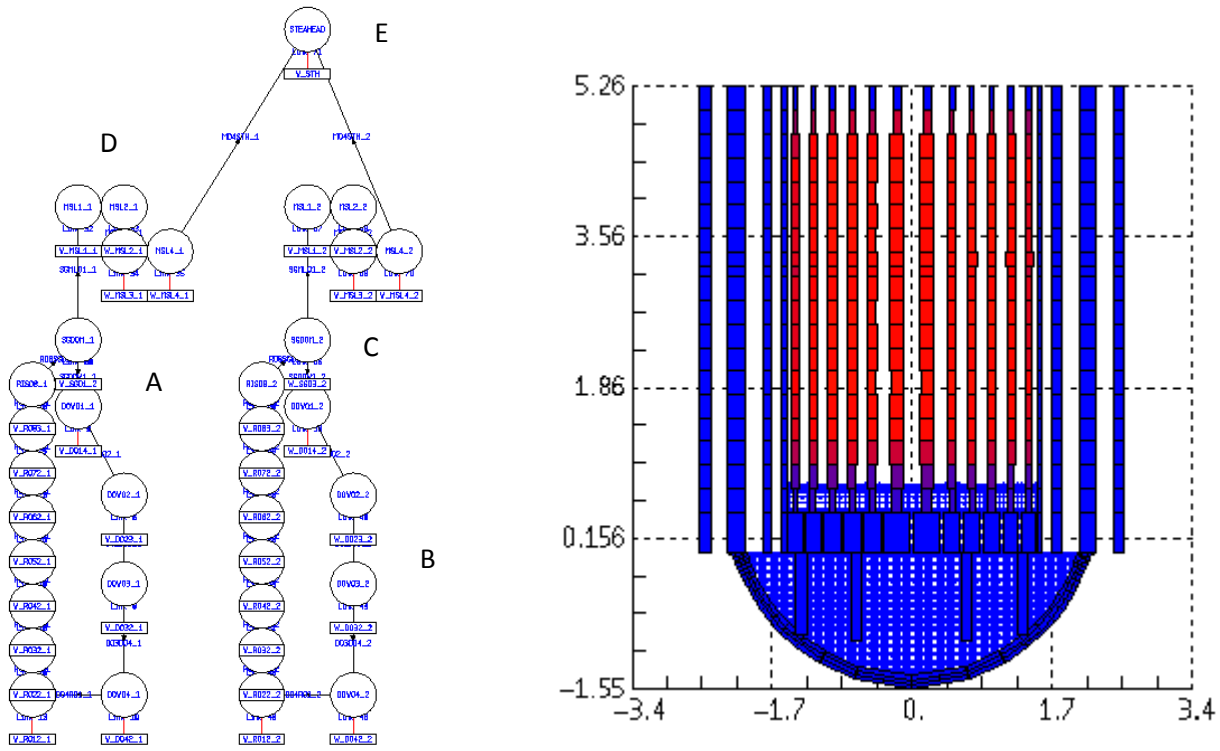

Figure 2 - a: *Secondary circuit nodalisation: A – Down comer, B – Riser tubes, C – Steam generator dome, D – Main steam line, E – turbine;* ***b:*** *ASTEC core modelling*

3. Scenario

In order to take into account the effect of time on the core degradation, this work considered a scenario, starting from a steady-state reactor of the AP 1000 at power conditions (3415 MWt). In particular, it has been chosen for presentation of the results and discussion a severe accident of type LOCA. The breach is located on the cold leg with a section of $0.018241 m^2$. The SA sequence considers the intervention of some passive security systems as Reactor Water Makeup Tanks (RWMT) and the accumulators, but not consider the flow from the In-containment Refueling Waters System Tank (IRWST) which would ensure the core cooling.

4. Simulation model

A comprehensive analysis of the nuclear reactor during the transient evolution for the LOCA event with cooling (Accumulators and RMST) is presented in this section. The studied scenario is a loss of coolant accident (LOCA) due to a breach on the cold leg in the primary circuit: the pressure drop causes the signal to activate isolation of main steam line and the reactor scram occurs. Subsequently, thermal power decreases, and so the water level in the vessel, the pressure in the dome, the steam flow, the feed-water flow and the mass flow rate in the core. The closure of the Main Steam Isolation Valves (MISVs) moreover determines the trip of the feed-water turbine pumps. The reactor collapsed level drops dramatically activating the emergency core cooling systems that consist in this case in two accumulators and two Core Makeup Tanks (CMT). The CMT is a passive high pressure system that is actuated when the pressure in the circuit decrease below 148 bar while the accumulator needs the pressure to decrease below 48 bar to start working. Anyway these systems do not provide core cooling for a long time, and after 500 seconds the valves of IRWST fail, and the core water level decreases sharply.

5. IVR Simulation

The ASTEC code cannot simulate the flood effect due to the IVR severe accident management strategy around the vessel: the RUPUICUV module indeed does not consider thermal-hydraulic phenomena and start to work only after the vessel failure. In this work, the flooding of the cavity was model as a heat sink imposing a determinate quantity of heat removing that can vary in time as boundary condition. having care to not exceed the critical heat flux (CHF) at the lower head wall. The CHF has been computed using the experimental correlation [6]:

$$q''_{CHF} = 1.44 \times (A + B\theta^2 + C\theta^3 + D\theta^4 + E\theta^5)$$

where the coefficients A through E are based on experimental results (W/m^2) for AP600 and θ is the lower head angle in degrees. The CHF value for AP1000 has been increased of 30% [6]. The CHF depending on the configuration of the molten pool - which in its turn depends on the time of core relocation to the lower plenum – it is possible to retrieve information on the spatial distribution of the decay heat, which is to be compared with the CHF. The assumed spatial distribution of the decay heat has been taken by a formula valid for a complete core relocation at a time around 3-4 hours, with a total thermal power of about 38 MW, which is compatible with the considered scenario.

Figure 3 shows the ratio between the heat flux used in this work and the CHF. At the bottom of the vessel (at 0°), the heat flux is the lowest, and also the CHF is the lowest. The ASTEC code requires the imposition of the total a constant power removed from the entire surface of the lower head. According to this, the value has been set so as to respect the constraint of the minimum value of the CHF on the lower head surface; it turns out that the heat flux has approaches the CHF at the bottom of the lower head, with the ratio q/q_{CHF} equal to around 0.8. At the top of the lower head (at 90°) where the CHF is higher, the value of the ratio results lower and equal to 0.25.

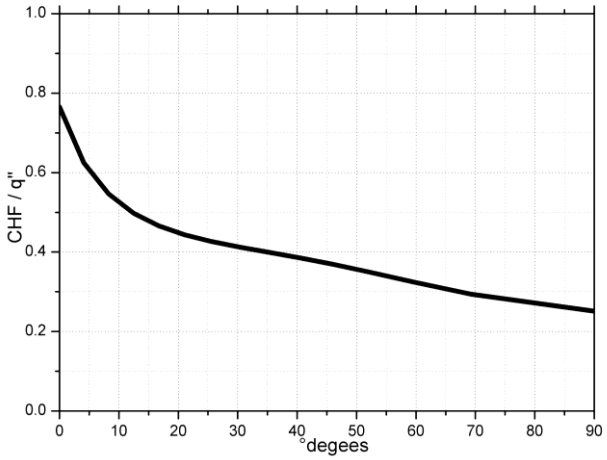

Figure 3 - *Ratio of the thermal heat flux to the CHF.*

6. Results and discussion

The simulation of the IVR retaining the molten core shows the temperatures in all the different sections of the vessel lower head remain below the steel melting one. With the only exception of the very bottom and top sections of the lower head, after a transitory phase where the heat removal is effective at low temperatures, the latter increase significantly, due to the presence of the magma facing the central sections of the lower head. This brings the inner layers of some sections to melting. At regime, the temperatures of all the sections of the lower head stabilize everywhere below 1000 K (figure 4).

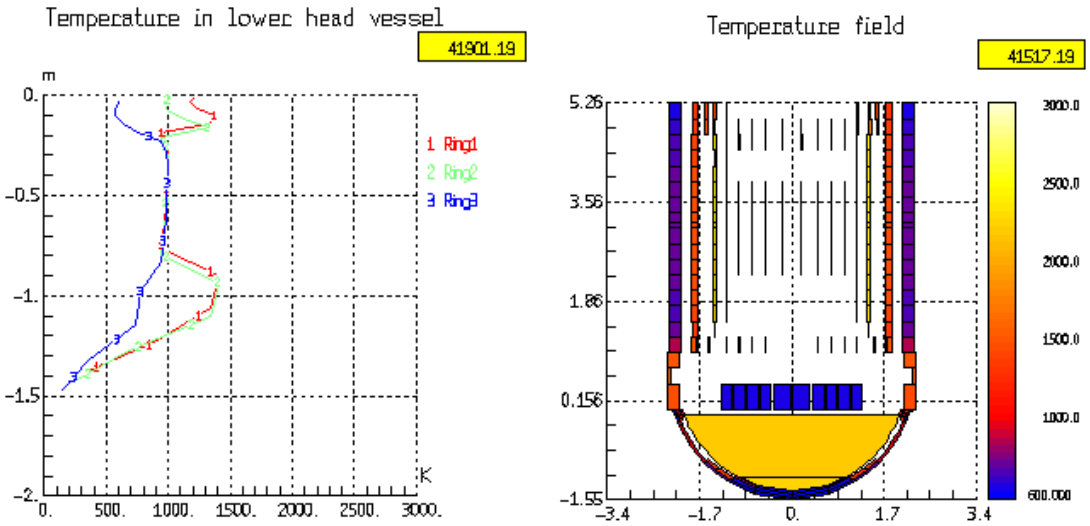

Figure 4 *– Temperatures in the different sections of the vessel lower head at regime (the curves for melted sections have remained frozen at the time of melting, without proceeding with the simulation), and status of the lower head.*

The right picture of figure 4 shows the graphical representation of the status of the lower head at the end of the simulation, from which it is possible to identify the molten layers.

7. Conclusions

The results of the simulation of the IVR with the ASTEC code reproduce the theoretical and experimental trends suggested by NRC: this fact might suggest the effectiveness of this core retention strategy. Anyway, further and more refined simulations are strongly envisaged to settle the odd behavior of vessel head wall temperatures, to cope with the setting of values that seem too high for still ensuring the heat exchange with water below the CHF.

8. Reference

[1] *ICARE user's manual for the integral code ASTEC V2.0"P. Chatelard, G. Guillard ASTEC-V2/DOC/09-03,Technical Note IRSN/DPAM/SEMCA 2009-147*

[2] *ASTEC-V1/DOC/07-18-ASTEC V1 CODE CESAR physical and numerical modeling Rev. 1 N. Trégourès, A. Moal*

[3] *Westinghouse AP1000 Design Control Document Rev.19 – Tier2-chapter 5- Reactor coolant System and connected systems. Section 5.4. Component and subsystem desig*n U.S.NRC 06-2011

[4] *Westinghouse AP1000 Design Control Document Rev.19 – Tier2-chapter 4- Reactor coolant System and connected systems. Section 4.5. Reactor material U.S.NRC 06-2011*

[5] *Westinghouse AP1000 Design Control Document Rev.19 – Tier2-chapter 6- Reactor coolant System and connected systems. Section 6.3. Passive core cooling systems. U.S.NRC 06-2011*

[5] *"Chemical Engineering design" Coulson & Richardson Fourth Edition volume. 6 Elsevier pg. 795*

[6] *NUREG/CR–6849- ERI/NRC-04-201 "Analysis of In-Vessel Retention and Ex-Vessel Fuel Coolant Interaction for AP1000".*

THE ROLE OF SIMULATION IN THE NUCLEAR POWER PLANT LIFE CYCLE

ROBERT BOIRE
L-3 MAPPS Power Systems and Simulation
8565 Côte-de-Liesse, Montréal, Québec, Canada H4T 1G5

ABSTRACT

Full Scope Simulators (FSS) have long been an indispensable part of the licensed training program for nuclear power plant control room operators. Traditionally, relatively complex and time consuming to create and validate and inextricably linked to the design and operational data of the reference plant that they reproduce, simulators have typically been planned as a single deliverable occurring relatively late in the plant design process. As a complete, integrated dynamic representation of the behaviour of a plant's process and control systems in their various states of operation, the value of upstream simulation for non-traditional applications such as initial learning, procedure development and verification, design verification and Human Factors Engineering is gradually being recognized. Nevertheless, the structured integration of simulation into the planning of the power plant design and training cycle has been somewhat slow. This paper looks at the opportunities for simulation in the entire plant life cycle and includes examples of experience from recent L-3 MAPPS projects in which simulation has played a wider role.

1. Introduction

Nuclear power plant simulation has traditionally focused on plant-specific Full Scope Simulators (FSS) with the primary objective being licensed operator training. The initial development and delivery of the vast majority of the FSS's has taken place either late in the plant construction cycle or following commercial operation. The development of an FSS has typically taken two to three years with a single integral delivery at the end of the project. The availability – or for that matter the need – for any kind of staged or incremental delivery of the evolving simulation or its use outside of operator training has been very limited.

The confluence of Nuclear New Build (NNB), widespread use of digital control systems (DCS's), powerful model development and training delivery tools and extremely inexpensive computation is leading to a paradigm shift in how and when simulations are created and used. In particular, the convergence of "simulation engineering" – the development and validation of an FSS by a simulator vendor and "engineering by simulation" towards leveraging the investment in model development has the potential of detecting latent design defects and thus reducing risk and optimizing plant design and cost.

2. Nuclear New Build

The primary requirement for FSS for NNB is that training starts between 12 to 24 months before fuel loading. This provides both a challenge and an opportunity for the FSS.

Figure 1 shows the schedule for the development cycle of a typical nuclear power plant and its associated FSS. The development of the FSS is inextricably linked to the design and operational data of the reference plant that it reproduces. Simulation of the plant process begins as much as 44 months before fuel loading. The primary challenge is related to the fact that the simulator development and in particular integration and validation takes place in parallel to the basic and detailed design of the DCS and well ahead of plant commissioning. Periodic updates following the actual plant commissioning and commercial operation typically take place 12 to 24 months after initial delivery.

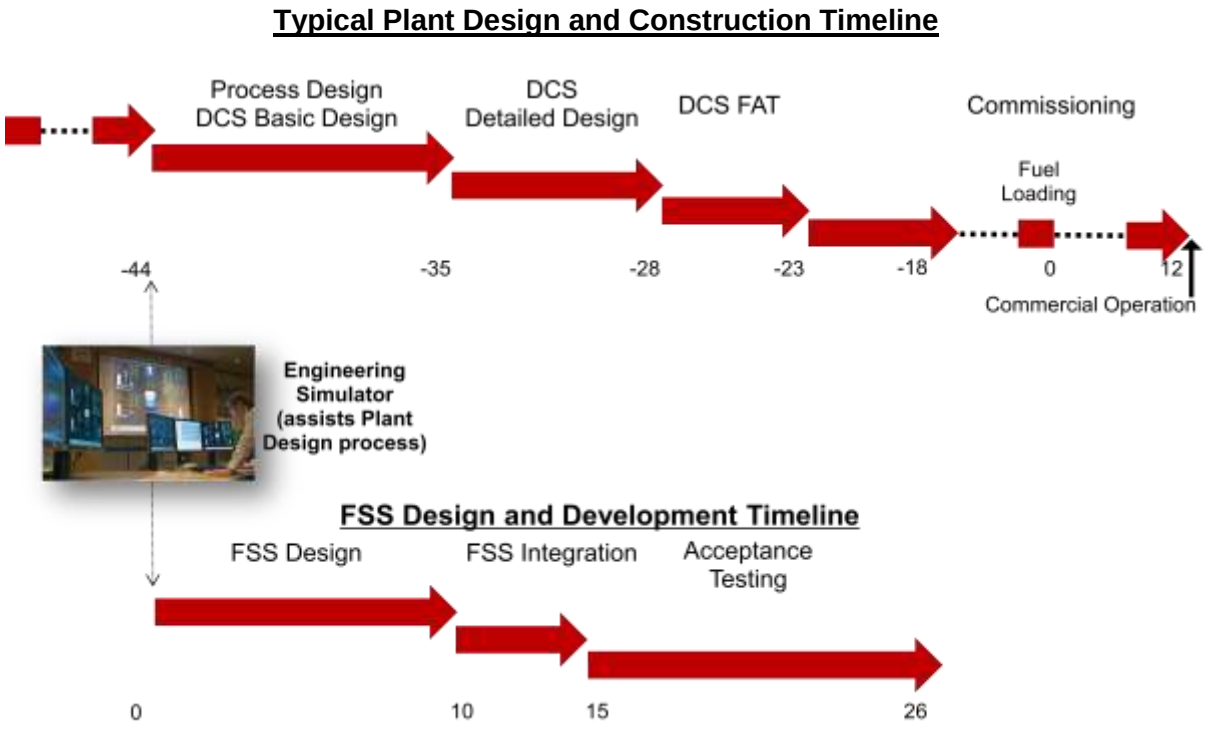

Figure 1: Plant and Simulator Development

There are consequences to this parallel development. These consequences include the fact that the plant detailed design is incomplete, that limited DCS verification and validation (V&V) has taken place at the time of FSS integration and that the turnaround time to solve plant design issues discovered during simulator testing can be long as it is driven by the plant schedule and the DCS supplier's quality process. The concept of a data freeze does not apply and change is inevitable during the FSS project and must be managed by the simulator developer. Above all, the simulator becomes a *de facto* V&V tool for plant design verification and virtual commissioning.

The opportunity is that this virtual commissioning through simulation can be a valuable tool for detecting and correcting latent errors that otherwise will need to be addressed during the actual commissioning of the plant (or later).

L-3 MAPPS experience with several new build programs (e.g. Olkiluoto 3 (OL3) (Finland), Ling Ao Phase II (China), Hongyanhe Phase I (China)) has shown that a large number of plant issues will in fact be detected during simulator testing. Typical issues include programming errors that are introduced during either the basic or detailed DCS design phases, inconsistent signal interfaces between different DCS products, between the control

system and plant components and inadequate parameterization at the time of simulator testing.

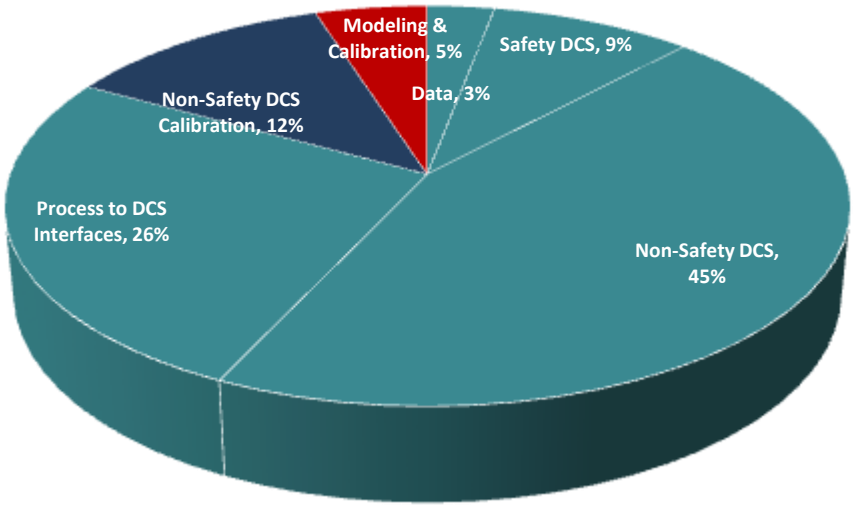

Figure **2** shows an example of the distribution of simulator discrepancies detected and resolved during testing of an L-3 MAPPS FSS for a NNB. As can be seen the vast majority of discrepancies are related to plant (rather than simulation) issues that would otherwise only be detected during actual plant commissioning and operation.

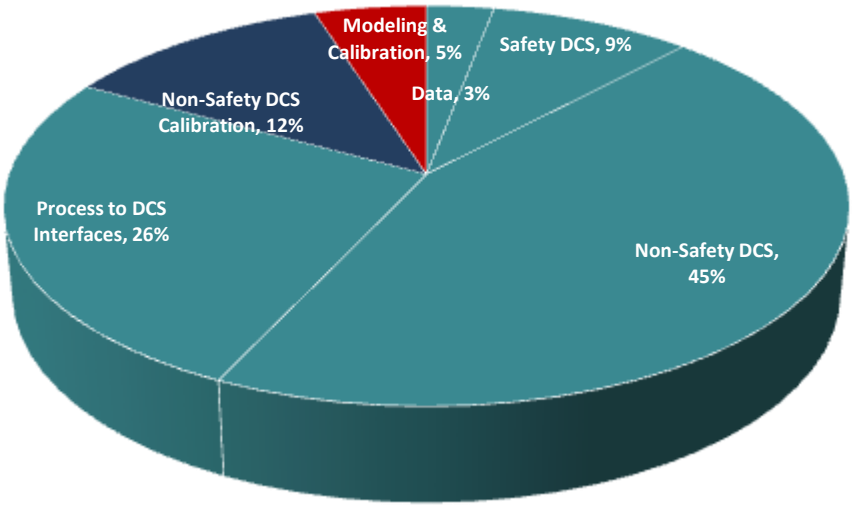

Figure 2: Distribution of Discrepancies Found during FSS Testing

Nevertheless, the effort required to discover, correct and validate the plant design changes by the plant or DCS vendor can have a harmful impact on the FSS schedule and the power plant owner's licensed operator training program. The means to mitigate this effect is that the virtual commissioning be part of the overall planning and development cycle of the plant. This requires that the simulator be considered within the big picture of the plant construction

schedule. By not doing so, the FSS development schedule and training will be compromised and the plant commissioning schedule is put at risk.

3. Engineering Simulation

Virtual commissioning is one example of the use of an Engineering Simulation (ES). One of the important criteria is the use of the same detailed, high-fidelity models of the plant systems that will eventually be developed for the FSS. Unlike the Nuclear Plant Analyzers of the 1990's which focused on primarily NSSS modelling and transient analysis, the ES relies on a plant model that is a complete, integrated, dynamic representation of the behaviour of all the plant systems controlled by the DCS (or DCS's) in their various states of operation. In fact, the primary difference between an ES and an FSS is simply a reduced hardware footprint and the absence of a need to fully reproduce the control room environment.

A second important criterion is related to the DCS itself. For the purposes of V&V, the implementation of the DCS in the simulator should ideally be based on running the same DCS application software that runs on the actual plant controllers. This requires a binary equivalent machine emulation (or virtual stimulation) from the DCS vendor (see [1] for a definition of DCS simulation techniques).

The use of a complete plant model allows a level of V&V that is not possible on a typical DCS test facility. It also allows the use of the ES for plant procedure development and validation. L-3 MAPPS has delivered the OL3 ES that is used for V&V testing and procedure development and validation.

Although the integrated ES described above has obvious advantages for V&V testing, there are two important disadvantages. The first is that the ES is available relatively late in the plant construction. This is partially because it has been derived from the FSS development and above all because the V&V testing can only begin once the detailed design of the DCS is complete and the DCS application software is available. The second is that there has been no prior, simulation-based opportunity to minimize discrepancies at either the system or basic design level before preparation of the DCS application software.

The solution is to perform incremental simulation-based testing on a system level in parallel to plant system design. This upstream integration of the ES into the plant design process makes it possible for simulation to achieve its full potential.

In this structured approach, each plant system and its associated controls and HMI are simulated starting from the availability of the basic design data. The individual simulations are used for standalone system level testing. Discrepancies are fed back into the plant or DCS vendor's design team for resolution and revalidation. This process provides early detection and limits accumulation of design errors into the integrated testing stage. The individual simulations are integrated into a plant model that can be used for eventual integrated V&V testing with either the DCS application software or even the actual I&C cabinets. The process in fact mimics the methodology traditionally used to build up a FSS but is applied to the plant design phase. The FSS in effect becomes a by-product of the plant engineering.

Though the benefits seem obvious, the industry has truly embraced the technology only in recent years. One reason is that simulators have traditionally been viewed as training devices with computational limitations. This is no longer the case. Another reason may be the perception that the data required for simulation will not be available soon enough to support early development of the individual simulations. In fact, the data that is required to start simulation of a particular system is the same data that is required to start the basic I&C design for the system. This essentially consists of the general system performance and

safety requirements and P&ID's. This information is generally found in the preliminary system design manuals. Generic component data can be used until such time as vendor data is available from the detailed design.

This strategy of continuous evolution of the simulation from system level to plant model to V&V simulator to FSS and data driven updates from basic design to equipment specification to DCS application software requires state-of- the-art configuration control mechanisms for the simulation toolset in order to ensure an efficient workflow. L-3 MAPPS' Orchid® simulation tools, and in particular the Orchid® Modeling Environment (Orchid® ME), is specifically designed to ensure configuration control. Orchid® ME is a client-server application designed to support large development workgroups working in a constantly changing environment. Orchid® ME includes many features that are unique among model builders including individual and shared workspaces, a check-in/check-out mechanism, versioning control over simulation schematics and component libraries, integrated source data referencing and validation, visual comparison tools for all sources including simulation schematics, support for geographically distributed workgroups and automated testing, data gathering and regression analysis features.

4. SOFIA

SOFIA (*Simulateur d'Observation du Fonctionnement Incidentel et Accidentel*) is an example of another ES with a different set of goals. SOFIA has been developed jointly by L-3 MAPPS, AREVA and the *Institut de Radioprotection et de Sûreté Nucléaire* (IRSN) [2, 3]. SOFIA includes separate simulations of four different types of French nuclear power plants including a Generation III+ EPR™. The SOFIA ES at IRSN is shown in

Figure **3**.

Figure 3: SOFIA at IRSN (source: Noak/Le bar Floréal/IRSN)

The simulators run within the Orchid® simulation environment and most of the models have been developed with Orchid® ME. Each simulation includes a plant model that supports a scope of simulated operations equivalent to an FSS. All the simulators include the CATHARE 2 code for modeling of the NSSS. CATHARE 2 is a system code for PWR safety analysis, accident management, definition of plant operating procedures and for research and development. It is also used to quantify conservative analysis margins and for licensing [4]. The EPR™ version also includes simulation of the core neutronics with Orchid® Core Builder. Unlike an FSS, SOFIA does not reproduce a specific control room environment but rather uses a DCS-like HMI interface that allows the user to carry out all procedures available to operators.

SOFIA serves both training and engineering functions. As a training simulator, it is used to provide training in elementary plant systems and operating strategies during incident and accident situations to design and commissioning engineers, nuclear safety authority inspectors and IRSN safety specialists. As an ES, it is used to perform studies related to complex accident sequences that require an overall plant model, to design and validate procedures, to support the safety analysis of planned plant modifications and to develop emergency procedures and drills.

A key technology difference between the OL3 ES and SOFIA is the use of a simulated (instead of an emulated version) of the DCS. This difference reflects the different objectives of the two simulators. The objective of the OL3 ES is the V&V of the actual DCS application software destined for the plant. One of the goals of SOFIA is validation of system design modifications at the basic design level, particularly in terms of control strategies, operating procedures analysis and improvement, preliminary safety analysis and plant engineering and emergency response training. In this case, a key requirement is the ability to rapidly develop and test alternate control strategies using Orchid® development tools and support for multiple software configurations.

5. Human Factors Engineering

Another example of where upstream simulation is playing a vital role is in Human Factors Engineering (HFE). The Center for Advanced Engineering Research (CAER) has set up a research facility that includes a Reconfigurable Main Control Room Simulator (RMCRS). It is specifically designed to support research into Generation III/III+ control room design, human factors studies for new power plants and digital I&C [5].

In this case a specific plant-referenced simulation is less important than a simulation that supports the full operating envelope including major transients that an operator may see. L-3 MAPPS has provided an EPR™ plant model with typical HMI displays that are used as the operator interface and the software tools that allow user to modify or test new displays. The RMCRS is shown in Figure 4. The simulator includes sophisticated eye tracking technology and the Observer XT event logging software from Noldus Information Technology for the collection and analysis of human performance data.

CAER's plan includes the study of the impact of I&C system failures on operator performance by interfacing an actual AREVA TELEPERM XS digital safety system to the plant model.

Figure 4: CAER Reconfigurable Main Control Room Simulator

Similarly Idaho National Laboratory (INL) is using simulators as part of the Human Systems Simulation Laboratory (HSSL) to develop and test newer digital control room designs especially in terms of digital control room upgrades of existing plants. INL is currently conducting research to support the upgrade of the main control room at the San Onofre Nuclear Generating Station (SONGS), a two-reactor plant operated by Southern California Edison Company. The existing SONGS simulator software, already using L-3 MAPPS' platform and models, will be complemented by L-3 MAPPS' Orchid® Touch Interface using touch-screen technology to provide a virtual representation of the control room hard panels. The software development tools will enable INL to create and study different panel prototypes. The prototypes will be evaluated using operator-in-the-loop testing, and basic operator performance principles will be disseminated to the industry. Utilities will then work

with their plant vendors to apply research-derived principles as design recommendations for their specific needs.

6. New Training Applications

Licensed operator training has traditionally used a combination of classroom fundamentals and procedure driven, FSS-based operations training. The industry is however facing the challenge of training an emerging, new generation nuclear workforce. Simulation can also be used upstream of operations training to facilitate understanding of the physical process and interactions that take place during power plant operation and transients. L-3 MAPPS is coupling 2D and 3D visualization technology and simulation to bring real-time, simulation-driven, animated physical systems allowing immersive, participatory learning in the classroom. The visualization can either be coupled to generic power plant simulation that provides fundamental training or to a FSS. The application of visualization with simulation as a new training application is discussed further in another paper presented at ENC 2012. [6].

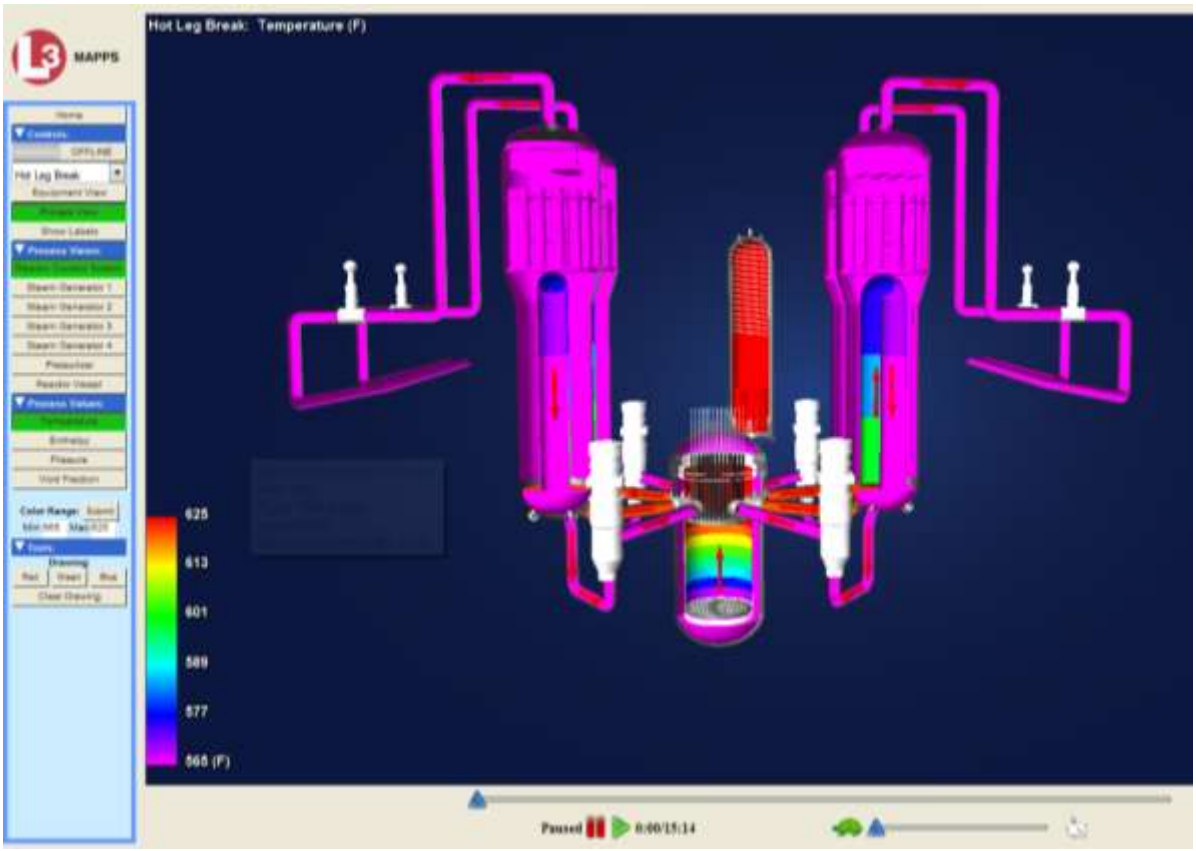

Figure 5: 3D Transient Fundamentals Trainer

7. Conclusions

FSS's have traditionally been used to deliver operations training. However, the accuracy and depth of today's models and the plant data that they encompass provide opportunities for leveraging the investment in the models for their use in engineering. The structured integration of simulation into the plant engineering process is a means of reducing cost and risk by integrating simulation-based V&V early into the development cycle. An efficient workflow requires simulation tools with start-of-the-art workgroup and configuration control features Simulation is also a means of providing fundamental learning to the new generation nuclear workforce through hands-on immersive visualization and learning.

8. References

1 http://www.mapps.l-3com.com/simulator-distributed-control-systems.html
2 Sepielli M., Negrenti E., Parisi C., Cappelli M.' "The Role of Thermal-hydraulic System Codes in NPP Engineering Simulators and the ENEA Strategy", Proceedings 20th International Conference Nuclear Energy for New Europe 2011, Bovec (Slovenia), 12-15 September 2011
3 http://www.irsn.fr/FR/base_de_connaissances/Installations_nucleaires/Les-centrales-nucleaires/Pages/simulateur-SOFIA.aspx
4 Cappon H., Dufeil Ph., Veilleux L., "Integration of the CATHARE 2 Safety Analysis Code on the SOFIA Engineering Simulators", Proceedings of 2010 PowerPlantSim Conference, San Diego (USA), 21-26 February 2010.
5 Carl Elks, et al. Design and Realization of a Configurable Main Control Room to Support Human Factors Research in Nuclear Power Plant Operations. 8th American Nuclear Society International Topical Meeting on Nuclear Plant Instrumentation, Control and Human-Machine Interface Technologies NPIC&HMIT 2012, San Diego CA, July 22-26, 2012.
6 Dimitri-Hakim R., "3D Visualization and Simulation to Enhance Nuclear Learning", Eurpoean Nuclear Conference, 9-12 December 2012, Manchester, United Kingdom.

STEADY STATE THERMAL HYDRAULIC OPERATIONAL PARAMETERS AND SAFETY MARGINS OF NIRR-1 WITH LEU FUEL USING PLTEMP-ANL CODE

S.A. JONAH, Y.V. IBRAHIM,

Centre for Energy Research and Training, Ahmadu Bello University,

P.M.B. 1014, Samaru-Zaria, Nigeria

M. KALIMULLAH, J.E. MATOS

Nuclear Engineering Division, RERTR Program. Argonne National Laboratory,

63490, Illinois, USA

ABSTRACT

The PLTEMP/ANL code version 4.1, 2011 was used to perform thermal hydraulic analysis of a miniature neutron source reactor (MNSR) facility with the proposed UO_2 LEU fuel core having 348 fuel pins in the core configuration and at a proposed nominal power of 34 kW for the determination of steady state operational parameters and safety margins. Measured data of NIRR-1 with the current HEU I core at the present nominal power of 31 kW was used to validate calculated data. Results show that the LEU margin to ONB, relative to nominal operating powers of 34 kW is substantially high and compares well with the corresponding margin for HEU core. Considering that the cladding material and the fuel for the proposed LEU core have higher melting points as well as higher resistance to corrosion, the safety margins for steady state operation are enhanced for the conversion of NIRR-1 in particular and MNSR in general.

1. Introduction

The PLTEMP/ANL series of code have been frequently used to perform thermal hydraulic analysis of research reactors for the determination of steady state parameters and safety margins [1]. The steady state parameters include fuel, clad, and coolant temperatures as functions of power. Safety parameters such as peak heat flux, the minimum critical heat flux (CHF), the minimum flow instability power ratio (FIR) and the margin to onset of nucleate boiling (ONB). The code also calculates radial and axial distributions of fuel, cladding, and coolant temperatures in a fuel assembly consisting of several coaxial fuel tubes cooled by light water or heavy water flowing in the annular gaps (i.e. coolant channels) between adjacent fuel tubes. To demonstrate the application of the code for the first time to calculate natural circulation flow rate in a reactor having solid fuels, the Nigeria Research Reactor-1 (NIRR-1) was modeled by the code. NIRR-1 is a Miniature Neutron Source Reactor (MNSR) designed by the China Institute of Atomic Energy (CIAE). The present HEU core of NIRR-1 is made up of 347 fuel pins with an enrichment of over 90 % and three Al dummy rods [2]. A detailed physics description of NIRR-1 has been provided in ref. [3]. Furthermore, neutronics analysis has shown that conversion to

LEU is feasible using UO_2 fuel enriched to 12.5% [4]. A comparison of main parameters of current HEU core and the proposed LEU core of NIRR-1 is given Table 1. In another development, the CIAE has designed and commissioned a variant of the MNSR. It is known as the In-Hospital Neutron Irradiator (IHNI) for boron neutron capture therapy (BNCT) applications and has been designed from scratch to use LEU UO_2 fuel [5]. This paper presents preliminary results of reactor thermal-hydraulic performance and steady state safety analyses for conversion of NIRR-1 from the use of HEU fuel to the use of UO_2 LEU fuel. The objective of this work was to show that it is feasible to use the UO_2 fuel element that could safely replace the current HEU fuel.

	HEU	LEU
Type	Tank-in-pool	Tank-in-pool
Nominal core power (kW_{th})	31	34
Coolant/Moderator	De-ionised light water	De-ionised light water
Loading of U-235 in core (g)	1006.65	1357.86
Reflector	Metallic beryllium	Metallic beryllium
Excess reactivity - cold, clean (mk)	3.77	4.02
Neutron flux at inner irradiation sites	1×10^{12} $cm^{-2}s^{-1}$, stability $\pm$ 1%, horizontal and vertical variation < 3%	1.04×10^{12} $cm^{-2}s^{-1}$, stability $\pm$ 1%, horizontal and vertical variation < 3%
Number of irradiation sites	10 sites (5 inner and 5 outer)	10 sites (5 inner and 5 outer)
Core reactivity temperature coefficient	-0.1 mk/^{o}C; for core temperature 15-40 ^{o}C	-0.1 mk/^{o}C; for core temperature 15-40 ^{o}C

Table 1 A comparison of the main specifications of the HEU core and proposed LEU core of NIRR-1

2. Materials and Method

NIRR-1 is a low-power, tank-in-pool reactor with a nominal thermal power of 30 kW under steady state condition. It is sited at the Centre for Energy Research and Training, Ahmadu Bello University, Zaria, Nigeria and is one of the commercial MNSR facilities. The reactor core is a square cylinder of dimensions 23 cm by 23 cm and it is surrounded by Be annulus on the sides and a Be plate at the bottom. A tray for shimming the reactor in the event of reactivity loss due to Sm poison sits on top of core. The fuel elements are pin types and are arranged in a bird cage, consisting of 350 lattices for the fuel pins. A single control rod made up of Cd material in stainless steel cladding moves centrally inside a guide tube located at the centre of the core.

The whole core configuration sits in light water which serves as both coolant and moderator. The core is designed to be under-moderated with the number of $H/^{235}U$ ratio as 197 for the commercial MNSR. Thermal-hydraulics characteristics of HEU core stems from the use of $U\text{-}Al_4$ as fuel. The fuel type has a low linear power density of about 3.8 W/cm, which is comparable to that of power reactors [6]. The choice of the fuel meat provides a high value of thermal conductivity, while natural convection is adopted for cooling. Figure 1 shows a cartoon of the reactor.

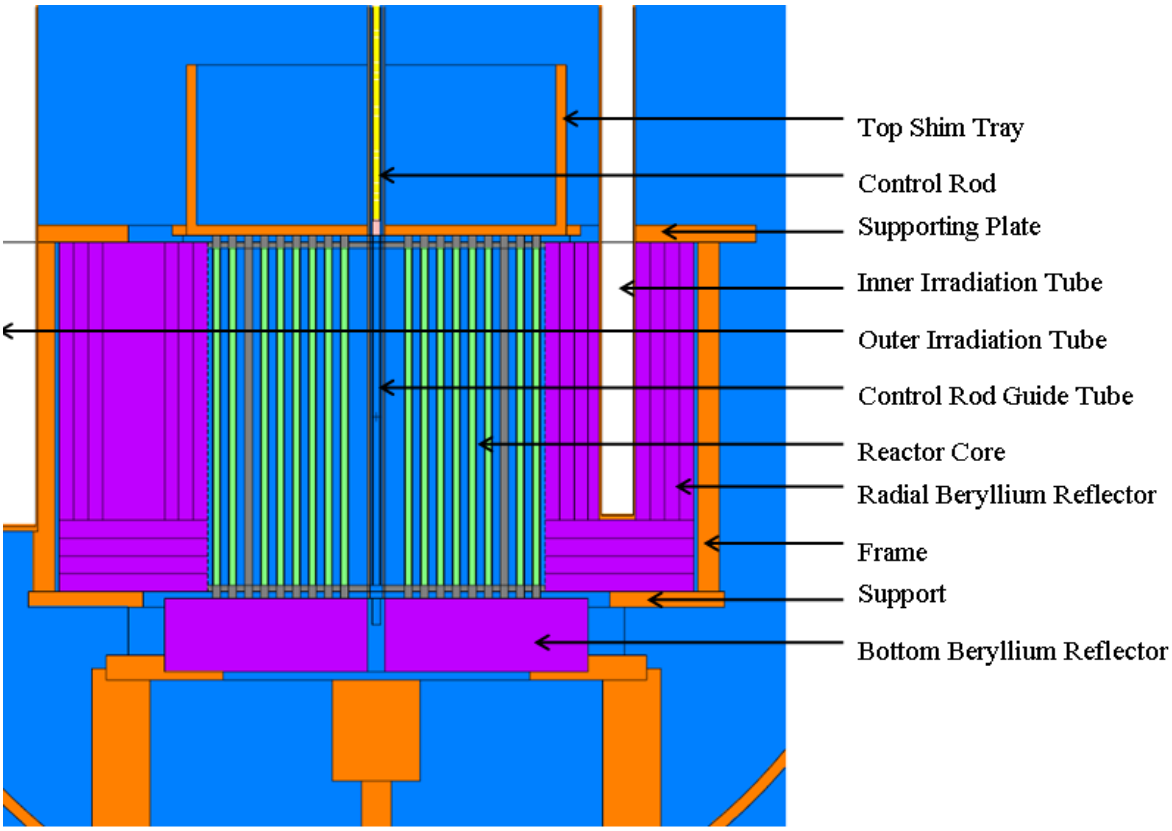

Fig.1 A close Side View of the NIRR-1 HEU Core configuration

PLTEMP/ANL is descended from the original PLTEMP code and was created to obtain a 1-dimensional steady-state temperature solution for a reactor core consisting of a group of nuclear reactor fuel assemblies, each comprised of multiple flat plates separated by coolant channels. The thermal conductivity of a variety of uranium-aluminum alloy fuels can be obtained from interpolation or from fitted equations. A series of calculations could be performed in one run to span a desired range of pressure drops. Some adjustments to the code were made for application to MNSR facilities to calculate the natural circulation flow rates and the code convergence. The number of coolant channels in the fuel assembly is always one more than the number of fuel tubes. This difference is required in the code input data. The innermost boundary of the first channel and the outermost boundary of last channel are assumed to be adiabatic in the multi tube radial heat transfer model of the code. Therefore in order to make use of the

existing provision, an artificial coolant channel of negligible radius (e.g. 1.075 mm) was created in the solid fuel rods used in MNSR facilities as shown in Fig 2. The dimensions of unit cell in Fig.2 are displayed in Table. To improve the code convergence, the outer iteration relaxation factors ε and the inner relaxation factor Finner were made part of the input data via inputs EPSLN and EPSNI on card 500 so that the user could adjust them as needed for convergence. Specific adjustments made in modeling NIRR-1 include the division of the 350 fuel/clad lattices into 24 type of fuel assemblies with 23 of them consisting of 15 fuel pins each and the 24^{th} assembly with 2 or 3 fuel pins respectively for the HEU and LEU cores. Calculations were performed using Bergles-Rohsenow boiling correlation option for water over the pressure range 1-138 bar, which includes the MNSR operating pressure range with the iteration option, ITRNCHF enabled.

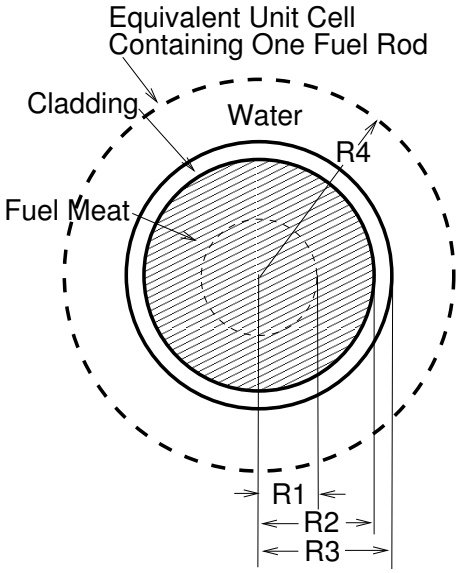

Fig. 2. PLTEMP/ANL Model of NIRR-1 HEU Core Fuel Pin

	Radius, mm
R1	1.075
R2	2.15
R3	2.75
R4	6.2167

Table 2 Dimensions of the unit cell show in Fig. 2

The reactor design data taken from ref. [7] was used in the safety margin calculations and are summarized in Table 3. The power distributions in the HEU and LEU cores of NIRR-1 were calculated using the MCNP5 code. The axial power profiles of the peak and average power fuel pins in the HEU and LEU cores were obtained from neutronics data. The hydraulic resistance of the coolant flow circuit in the PLTEMP/ANL model was obtained by calibrating the model to reproduce an experimentally measured coolant temperature rise of 13 ℃ (from 24.5 ℃ to 37.5 ℃) at a reactor power of 15 kW from measurements [8]. The results of this calibration for both reactor cores are also given in Table 3. Using the calibrated model, the coolant inlet temperature was raised and adjusted to get an outlet temperature of 70 ℃ in steady-state at the nominal reactor power. Table 3 also shows the adjusted inlet temperature and some operating parameters found by this calculation

3. Results and Discussion

Results in Table 4 show that measured data for current HEU core compare well with calculated data obtained by the PLTEMP code. Data are presented for operation at full powers, 31 kW and 34 kW respectfully for the current HEU core and the proposed LEU core. The calculated thermal hydraulic steady state operational characteristics and safety margins for NIRR-1 with the proposed UO_2 LEU fuel in the Table compare well with HEU data. The power at which ONB occur has been examined for the LEU fuel configuration and compared with the corresponding margins for the HEU fuel configuration. The results obtained were deemed more conservative and can be seen in the Table. The power level at which ONB occurs was calculated to be 65.2 kW and 67.8 kW respectively for the HEU and LEU cores. As can be seen, the prediction is far above the maximum operating power levels for the two cores. The maximum temperature of 113.2 ℃ at the surface of the zircaloy cladding for the LEU fuel is far below its melting temperature of 1850 ℃. Similarly, the maximum temperature of 147 ℃ at the fuel centerline is far below the melting temperature of 2865 ℃ for UO_2 fuel. At power levels above ONB, calculations have shown that the reactor would operate in the sub-cooled boiling regime until Onset of Significant Void (OSV) occurs at a power level of ~ 145 kW. The critical heat flux (CHF) would be reached at a power level far above that at which OSV is predicted to occur. Overall, these analyses show that the steady state thermal-hydraulics safety margins for the proposed LEU design compare with the HEU data and still satisfy technical specifications. Considering that the UO2 fuel and zircaloy clad have higher melting points and better resistance to corrosion compared with the materials of the current HEU core.

Thermal-Hydraulic Data	HEU	LEU
Reactor Power	31	34
Number of Fuel Pins in Reactor	347	348
Peak Pin Power, W	99.66	113.19
Average Pin Power, W	86.96	97.70
Peak Pin/Average Pin Power Ratio	1.146 ±0.3%	1.1586 ±0.3%
Fuel Meat	U-Al alloy	UO_2
Uranium enrichment	90.2 %	12.5 %
Cladding Material	Al alloy	Zircaloy-4
Gas in Meat-Cladding Gap	-	He
Meat Radius, mm	2.15	2.15
Gas Gap Thickness, mm	-	0.05
Cladding Thickness, mm	0.6	0.6
Fueled Length, m	0.230	0.230
Unheated Length Below the Fueled Length, m	0.009	0.009
Unheated Length Above the Fueled Length, m	0.009	0.009
Total Height of a Fuel Pin, mm	0.248	0.248
Inner Diameter of Annular Beryllium Around All Fuel Pins, m	0.231	0.231
Fuel Meat Thermal Cond., W/m-C	140	5.78
Cladding Thermal Cond., W/m-C	180	14.74
Gap Gas Thermal Cond., W/m-C	-	0.1767
Gap Thermal Resistance, m^2-C/W	-	~ 0.000283
Hydraulic Diameter for Hot Pin, m	0.0231	0.0231
Flow Area for Hot Pin, m^2	9.978E-5	9.978E-5
Depth of Water Above Core Top, m	4.7	4.7
Pressure at Core Top, MPa	0.1468	0.1468
Calibration of Hydraulic Loss Based on a Test at 15 kW:		
Core Inlet Temperature, ℃	24.5	24.5
Coolant Temp. Rise, ℃	13	13
Calibrated Loss Coefficient	67.3	68.6
Calculated Core Flow Rate, kg/s	0.277	0.277
Steady-State at Nominal Reactor Power with Core Inlet Temp. Adjusted to Get an Exit Temp. of 70 ℃:		
Adjusted Inlet Temperature, ℃	53.78	52.28
Core Flow Rate, kg/s	0.441	0.47
Coolant Outlet Temperature, ℃	70.0	70.0
Max. Cladding Surface Temp., ℃	86.4	87.8
Max. Fuel Centerline Temp., ℃	86.7	100.5

Table 3 Thermal Hydraulic Analysis of NIRR-1 Using PLTEMP/ANL Code

Parameters	HEU Core at 31 kW		LEU Core at 34 kW
	Measured	PLTEMP	PLTEMP
T_{out} (^oC)	45.2	44.13	36.93
T_{clad} (^oC)	-	112.7	112.7
Reactor Power at ONBR=1 on Peak Pin Without Hot Channel Factors	-	65.2	67.8
CORE FLOW (Kg/s)	-	0.586	0.586

Table 4 Comparison of Measured and Calculated Steady State T-H Data and Safety Margins for NIRR-1

4. **Conclusion**

A PLTEMP/ANL model of the current HEU core configuration of NIRR-1 was developed to perform the analyses of the thermal-hydraulic characteristics of the reactor operating at steady state. Calculated for the present HEU core obtained agree well with measurements from the SAR [2]. Consequently, the HEU core was replaced with the proposed UO_2 LEU core in order to evaluate the impact of conversion on the steady state thermal hydraulic safety margins. Data obtained show that the maximum cladding surface temperature, centre line temperature and the margins to ONB of the LEU fuel agree well with the corresponding values for the HEU core. The results show that the LEU margin to ONB, relative to nominal operating powers of 34 kW is substantially high and compares well with the corresponding margin for HEU core. Similarly, the predicted clad surface and fuel temperatures for the proposed LEU cores are comparable with the corresponding data for the HEU core. Considering that the cladding material and the fuel for the proposed LEU core have higher melting points as well as higher resistance to corrosion, the safety margins for steady state operation are enhanced for the conversion of NIRR-1 in particular and MNSR in general.

5. Acknowledgements

This work was supported by the IAEA Coordinated Research Project No.NIR/13934 entitled “Conversion of MNSR from HEU to LEU” and Research Agreement, Contract No 1F-30204 UCHICAGO ARGONNE, LLC (Operator of Argonne National Laboratory)

6. References

1. A. P. Olson and M. Kalimullah, "A Users Guide to the PLTEMP/ANL V4.1 Code," Global Threat Reduction Initiative (GTRI) – Conversion Program, Nuclear Engineering Division, Argonne National Laboratory, Chicago, IL, USA (April 5, 2011).
2. Nigeria Research Reactor-1: Final Safety Analysis Report, Centre for Energy Research and Training, Energy Commission of Nigeria, Ahmadu Bello University, Zaria, CERT/NIRR-1/001, August 2005.
3. Jonah S.A., Liaw J.R., Matos J.E., 2007. Monte Carlo simulation of core physics parameters of the Nigeria Research Reactor-1(NIRR-1)" Annals Nucl. Energy 34, 953-957
4. Jonah S. A., Ibikunle K., Li Yi-guo. "A feasibility study of LEU enrichment uranium fuels for MNSR conversion using MCNP" Annals of Nuclear Energy, 36 (2009), 1285 –1286
5. Li Yi-guo, "The Physics Experimental Study for In-Hospital Neutron Irradiator (INHI)", Proc. International Meeting on Reduced Enrichment for Research and Test Reactors, Prague, Czech Republic, 23-27 September 2007
6. Shi Shuangkai, "MNSR Thermal Hydraulics", part of MNSR Training Manual, p. 10, China Institute of Atomic Energy, unpublished, 1993.
7. Ampomah-Amoako E., Akaho E. H. K., Anim-Sampong S., Nyarko B.J.B., "Transient Analysis of Ghana Research Reactor-1 using PARET/ANL Thermal Hydraulic Code," Nucl. Eng. and Design, Vol. 239, pp. 2479-2483 (2009)
8. Ahmed Y.A., Balogun G.I., Jonah S. A., Funtua I. I., "The Behavior of Reactor Power and Flux Resulting from Changes in Core-Coolant Temperature for a Miniature Neutron Source Reactor," Annals of Nuclear Energy, Vol. 35, pp. 2417-2419 (2008).

CFD ANALYSIS OF AIR-WATER TWO-PHASE FLOW IN A HELICALLY COILED TUBE

M. COLOMBO, A. CAMMI, J. DE AMICIS, S. LORENZI, M.E. RICOTTI
Politecnico di Milano, Department of Energy, Nuclear Engineering Division-CeSNEF
Via La Masa 34, 20156, Milano, Italy

ABSTRACT

Helically coiled tubes represent a valuable solution to improve the performance of nuclear reactor Steam Generators (SGs), as they are very attractive for Small-medium Modular Reactors (SMRs) of Generation III+, which require in particular compactness as all the primary system components are located inside the reactor vessel.
In this paper, the two-phase flow of an air-water mixture in a helically coiled pipe is investigated with the Computational Fluid Dynamic (CFD) code ANSYS FLUENT. In particular, the two fluid Eulerian model implemented in the code is applied in the simulations. As the CFD simulation of two-phase flow is a very challenging subject, a preliminary validation is made by comparison with experimental measures of frictional pressure drop and void fraction available in literature. Particular attention is devoted to the settings and parameters that considerably affect the results of the simulations. The diameter of the dispersed phase, in particular, turns out to be a key parameter for the accuracy of the results.
Despite some drawbacks, results are fairly accurate as time average values of the void fraction and the frictional pressure drop show satisfactory agreement with the experimental data. In addition, the code seems to catch the effect of the centrifugal force introduced by tube bending on the two-phase flow structure.

1. Introduction

Helical pipes provide better heat transfer characteristics, a significant enhancement of the critical heat flux, an improved capability to accommodate the thermal expansion and a higher compactness of the component design with respect to straight pipes [1]. In the nuclear field, they are of particular interest for Small-medium Modular Reactors of Generation III+, where all the primary system components are located inside the reactor vessel.
This paper presents the Computational Fluid Dynamic (CFD) study of the two-phase flow of an air-water mixture inside a helically coiled pipe, studied through the ANSYS FLUENT 14.0 code [2]. Two-phase CFD is also increasingly applied in the nuclear field, as a promising way to extend the simulation capabilities for many nuclear reactor thermal hydraulic issues [3].
While for single-phase flow in helical pipes several authors have performed detailed numerical simulations with different computational schemes and turbulence models, publications available on the numerical simulation of the two-phase flow in helical tubes are rather limited, due to the important modelling complexities. Jo et al. [4] numerically investigated the two-phase flow heat transfer in helical tubes of a pressurised water reactor steam generator using a CFX code. They reported the formation of a liquid film on the outer side of the helix and showed good agreement with experimental data. Jajakumar et al. [5] presented a CFD analysis for heat transfer to air-water two-phase mixture flowing through a helically coiled heat exchanger. Chandratilleke et al. [6] made an investigation on flow boiling in curved pipes with a non-equilibrium model based on the Eulerian multiphase approach.
In this paper, the adiabatic flow of an air-water mixture is simulated with the ANSYS FLUENT 14.0 code to study the effect of the geometry on the flow field and the phase distribution, in order to verify the possibility to have accurate predictions of the void fraction and the frictional pressure drop, through comparison with experimental data.
Usually, physical quantities as the void fraction or the frictional pressure drop are estimated with correlations and a number of them are available also for the helical geometry [7-10]. Although some of them show a great accuracy, they are unavoidably related to the experimental set of data used for their development, as all include some empirical coefficients fitted to experimental data. As a consequence, it is not easy to find a correlation appropriate for a wide range of geometrical and operating conditions, in particular for the

two-phase flow. Therefore, the great opportunity of having a numerical tool able to predict with a great accuracy the void fraction and the frictional pressure drop without make reference to a particular geometry or a limited range of operating conditions.
In this paper the comparison is limited to an adiabatic air-water flow. The simulation of the air-water mixture takes advantage of a larger availability of experimental data in the literature, in particular for the void fraction. The availability of experimental data is in fact reduced when the steam-water mixture or higher system pressure conditions are addressed. In this respect, the availability of accurate numerical predictions could also mitigate the shortage of experimental data in some particular situations. In this paper, the data of Akagawa et al. [11] are used for comparison, since they are related to both the void fraction and the pressure drops.
Firstly experimental data of Akagawa et al [11] are briefly discussed and then CFD model and settings are presented. The fundamental effect of the diameter of the dispersed phase is also discussed in the paper. Finally, results and comparison with experimental data are presented.

2. Experimental data

Experimental data used for the purpose of the present work are taken from Akagawa et al. [11], who studied experimentally the flow pattern, the void fraction and the pressure drop behaviour in a two-phase air-water flow through helically coiled tubes, comparing their results with those obtained with straight pipes. The considered tube diameter *d* is 9.93 mm with a *d/D* ratio of 1/11 and 1/22.7, where *D* is the diameter of the helix. The tests were performed by imposing a fixed flow rate for the liquid phase and then varying the air flow rate, measuring the void fraction and the pressure drop, while the flow pattern was obtained by direct visualization of the fluid flow. The range of water superficial velocity is from 0.35 m/s to 1.16 m/s, while the gas superficial velocity goes from 0 m/s to 5 m/s.
For the comparison between experimental data and computational results, only data from the first coil (d/D=1/11) are considered, with a fixed liquid superficial velocity j_w=0.85 m/s and increasing values of the air superficial velocity j_a, in order to study the range of void fraction from 0 up to about 0.7.

3. CFD Model

The CFD simulations were made with the ANSYS FLUENT 14.0 code [2]. The Eulerian multiphase model implemented in the code was adopted for the simulation of the air-water two-phase flow. The Eulerian model describes the multiphase flow as interpenetrating continua, where the space occupied by each phase is described by the volume fractions and momentum and continuity equations are solved for each phase.
An adiabatic air-water mixture was simulated, neglecting phase change and heat and mass transfer between the phases. Fluid properties were also considered constant during the simulation (Table 1). Momentum transfer between the phases was accounted for by a proper drag force term in the momentum equation, calculated with the universal drag law available in the FLUENT code.
ANSYS FLUENT uses an interaction term between the phases in the momentum equation of the following form, for phase 1:

$$\overline{R}_{21} = K_{21} \cdot \left(\overline{v}_2 - \overline{v}_1\right).$$

The secondary phase (phase 2) is assumed to form droplets or bubbles. The exchange coefficient K_{21} for the interfacial exchange term is written in the following form:

$$K_{21} = \frac{\alpha \cdot \left(1-\alpha\right) \cdot \rho_2 \cdot f}{\tau_2},$$

where α is the void fraction, ρ_2 the density of the dispersed phase, *f* the drag function, calculated with the universal drag law, and τ_2 the "particulate relaxation time", which reads:

$$\tau_2 = \frac{\rho_2 \cdot d_p^2}{18 \cdot \mu_1}.$$

d_p represents the diameter of the bubbles or droplets of the dispersed phase, whereas μ is the viscosity of the continuum phase. More information could be found in [2].
All other interfacial force terms have been neglected. The k-ε turbulence model was used to simulate the turbulent flow, together with the standard wall function for the treatment of the near wall region. Pressure-velocity coupling was resolved using the Phase Coupled SIMPLE scheme; momentum and turbulent quantities were discretised with the second order upwind scheme, while the QUICK scheme was used for the volume fraction.

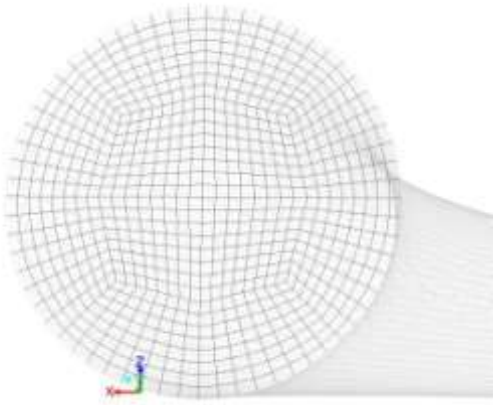

Figure 1 Mesh adopted for the simulations.

Table 1 Geometrical data and fluid properties.

coil diameter [m]	0.109
pipe diameter [m]	0.00992
helix angle [°]	2.5
water density [kg/m^3]	998.2
air density [kg/m^3]	1.225
water viscosity [Pa*m]	0.001
air viscosity [Pa*m]	$1.79*10^{-5}$
surface tension [N/m]	0.0727

A convergence criterion of 10^{-5} was applied for velocities, volume fraction and turbulent quantities. For a single experimental condition, a first simulation was made with a geometry including three turns of the helix, to reach developed flow conditions starting from a homogeneous mixture at the inlet of the pipe. For these simulations, a coarser grid was used. Outlet velocity and void fraction profiles were then applied as inlet conditions in successive simulations of short pipe sections made with a finer mesh. A structured mesh was used with 768 elements in the pipe cross section (Figure 1), for a total of 153600 hexahedral cells in a pipe length of about 8.5 cm. Different consecutive pipe sections were simulated. The number of mesh elements was selected following a grid independence study. Simulations were made in the time domain. Following the transient and the reaching of stationary conditions, physical quantities were evaluated as time average over an appropriate time interval.

4. Influence of the dispersed phase diameter

A large number of different parameters characterize the CFD simulation of the two-phase flow, making it a very challenging subject. One of the most important and sensitive parameter was identified after the first set of simulations to be the diameter of the dispersed phase, which plays a significant role in the calculation of the interfacial drag force term and has a great influence on the simulation results. A preliminary calibration of its value permitted to define the value d_p=0.1 mm as a reasonable value for a correct simulation of the air-water flow. Figure 2 shows the behaviour of the void fraction on the pipe cross section in a low flow quality case. In more details, a higher diameter value originates a weaker interaction between the two-phases, resulting in a clear separation between air and water, a higher value of the slip ratio and an extremely low value of the air volume fraction, much lower with respect to the experimental data (Figure 3). Starting from d_p=0.5 mm, simulations were

characterized by increasing difficulties to reach stationary conditions, convergence problems and mass conservation errors. A lower diameter value, on the contrary, causes a stronger interaction between air and water, a higher value of the air volume fraction and consequently a lower value of the slip ratio (Figure 2), up to the reaching of homogeneous flow conditions.

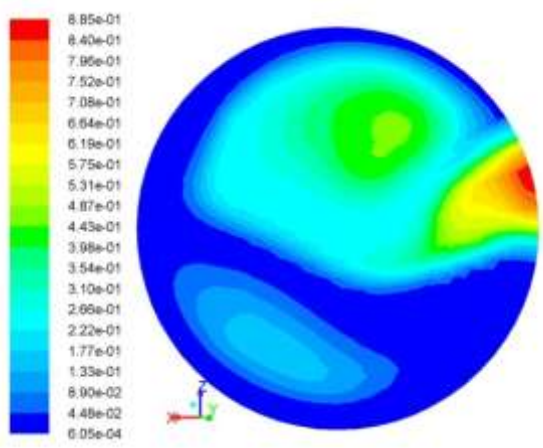

Figure 2 Void fraction profile on pipe cross section for j_w=0.85 m/s, j_a=0.164 m/s and d_p=0.1 mm.

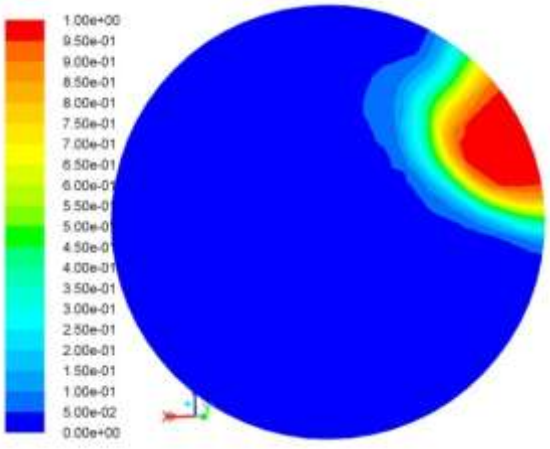

Figure 3 Void fraction profile on pipe cross section for j_w=0.85 m/s, j_a=0.164 m/s and d_p=0.5 mm.

5. Results and discussion

A validation of CFD results was made with a comparison with the data measured by Akagawa et al. [11] in the D=0.109 m helix at a fixed liquid superficial velocity j_w=0.85 m/s and for increasing air superficial velocities j_a. Simulated quantities were obtained as area averaged values on successive pipe cross sections. Reference values were calculated as a mean of the different area values belonging to stationary flow conditions. For the pressure drop, the difference between average pressures in two successive cross sections was considered.

A very good agreement between simulation results and experimental data is found for the air volume fraction (Figure 4). Only for the lowest flow quality the experimental data is underestimated; for the remaining points, the maximum deviation is 3.1 % and the Root Mean Square (RMS) error 2.14%. To enlarge the range of void fraction in the comparison, the final two points were compared with data at different water superficial velocity, showing higher but anyway satisfactory deviations.

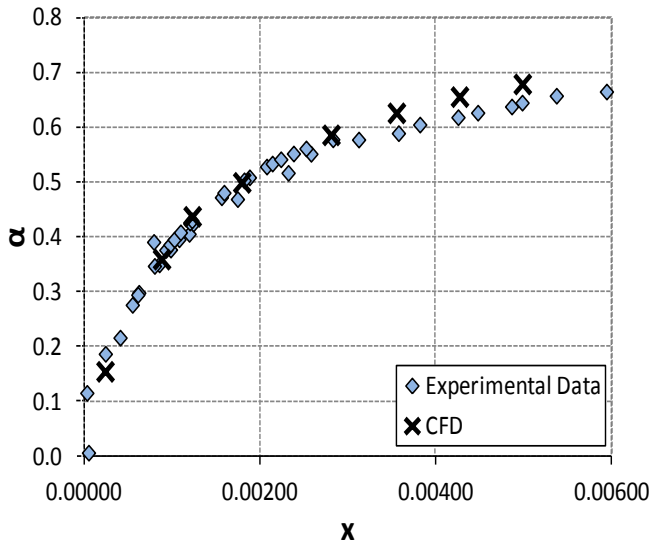

Figure 4 Comparison between experimental data and CFD void fraction results

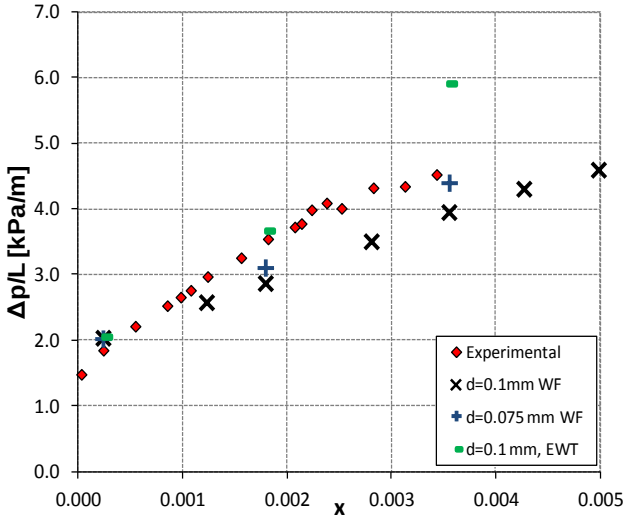

Figure 5 Comparison between experimental data and CFD frictional pressure drop results.

As concerns the two-phase frictional pressure drop, higher errors are observed, in particular for the higher values of the mass flow rate (Figure 5). In more details, the CFD model underestimates the pressure drop, with a RMS error of about 15% and a maximum deviation from experiments equal to 19%. All things considered, model behaviour can be considered quite satisfactory as a first calculation and in view of the many possible improvements.

A more detailed analysis of the effect of the dispersed phase diameter has underlined the possibility of improving the code pressure drop predictions with a small modification of its value. A value of d_p=0.075 mm permitted to better predict the frictional pressure drop in all the range of flow quality, reducing the RMS error under the 10%. As for the void fraction, the highest error corresponds to the lowest value of the flow quality (Figure 5).

Figure 6 shows the air void fraction profile and the phase distribution on a pipe cross-section. The effect of the centrifugal force is clearly visible, as the heavier water is pushed through the outer wall of the tube, while the lighter air phase occupies the inner wall region, causing the formation of a highly unsymmetrical flow pattern. Comparing two simulations made at different flow quality value, it is possible to underline the effect on the flow field of both centrifugal and gravitational forces. At low flow quality, the water is concentrated on the lower section of the cross section, although a liquid film on the tube outer wall is already visible, evidence of the fluid recirculation promoted by the centrifugal field (Figure 2). Increasing the air flow rate, the volumetric flow of the mixture is greatly increased, so the velocity of the two phases. As a consequence, the centrifugal force field predominates on the gravitational one and the interface between the phases is disposed along the vertical direction (Figure 6). These results find confirmation on the visual observations of the flow field provided in the work of Murai et al. [12].

The rather simple CFD model adopted (only the drag force has been considered for the interfacial momentum exchange between the phases) is able to satisfactorily reproduce the experimental data while catching the fundamental characteristics of the two-phase flow in the helical pipe. In particular, the errors are comparable or slightly better than the ones obtained with best correlations found in literature, when applied to their original data sets [7-10]. This suggests that it is the centrifugal force field that mainly influences the phase distribution and the interaction between the phases. At the lowest flow quality, on the contrary, the phase distribution and the interface structure are more complex and a dedicated model of the drag force and the interface interactions could be required to improve the accuracy of the simulations.

Additional simulations were made trying to obtain a more precise description of the near wall region with the FLUENT enhanced wall treatment, which solves the flow field all the way to the wall. A finer mesh was developed, made of 1024 elements in the cross section, refined in

the wall region (y^+~ 1-3). Air volume fraction in the channel cross-section is presented in Figure 7.
A more detailed description of the near wall region is shown, in particular for the liquid film attached to the wall. Void fraction data are in good agreement with experimental data, and no significant differences are found with respect to the previous case. The pressure drop is very well predicted at low-medium flow quality, unless they are overestimated at the highest quality value (Figure 5).

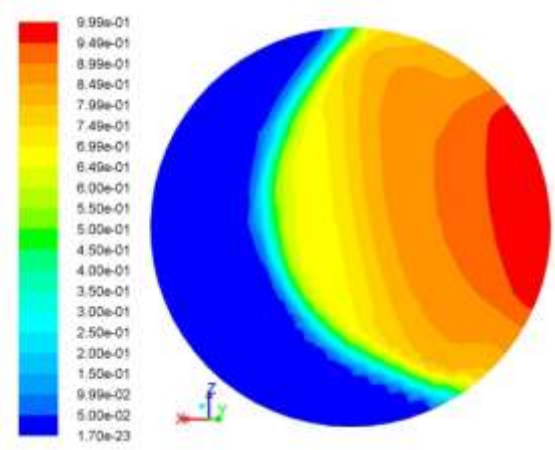

Figure 6 Void fraction profile on pipe cross section for j_w=0.85 m/s, j_a=1.253 m/s.

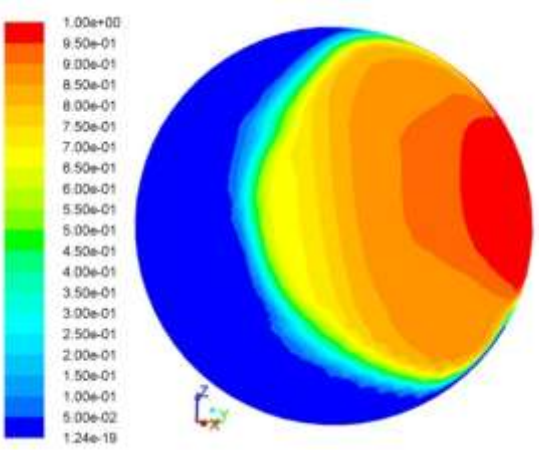

Figure 7 Void fraction profile on pipe cross section for j_w=0.85 m/s, j_a=1.253 m/s. Calculation was made using the enhanced wall treatment.

6. Conclusions

In this paper, the two-phase flow of an adiabatic air-water mixture in an helically coiled pipe is addressed through numerical simulation. In particular, the ANSYS FLUENT 14.0 package has been adopted. Simulation results were compared with experimental data available in literature, in order to explore the possibility to obtain reliable information about the void fraction and the frictional pressure drop. Different values of the flow quality were simulated by keeping fixed the water flow rate and increasing the air flow rate. Interaction between the phases is found to be strongly dependent on the diameter of the dispersed phase, whose value influences the void fraction and the configuration of the phases in the tube cross section.
The rather simple model adopted (only the drag force considered for momentum exchange between the phases) shows satisfactory results. RMS errors of 2.14% for the void fraction and less than 10% for the pressure drop were obtained. In addition, an analysis of the different models available for the simulation of the near-wall regions permitted to evaluate some differences especially in the predicted pressure drop and in the spatial configuration of the two phases.
Despite some drawbacks that require further investigation (dispersed phase diameter and near-wall treatment in particular), the CFD numerical simulations preliminarily proved to be a reliable tool for the prediction of void fraction and frictional pressure drops for an air-water two-phase flow in helical pipes. The obtained errors can be considered negligible or below the experimental uncertainty for the void fraction. Concerning the frictional pressure drop, accuracy of the results is comparable to the best correlations available in literature. Nevertheless, CFD simulations have the advantage not to make reference to a particular data set, which is required for the development of an empirical correlation.
Obviously additional validation is required, in particular to further support the applicability in a wide range of geometrical and operating conditions. Comparison with experimental data measured in different flow conditions and in helical pipes having a different coil diameter are foreseen in the near future, together with the simulation of steam-water mixture at higher pressures.

REFERENCES

[1]. A. Bejan, A.D. Kraus, Heat transfer handbook, Wiley, 2003.
[2]. ANSYS Fluent 14.0 User Guide.
[3]. D. Bestion, Applicability of two-phase CFD to nuclear rector thermalhydraulics and elaboration of Best Practice Guidelines, Nuclear Engineering and Design, http://dx.doi.org/10.1016/j.nucengdes.2011.08.068.
[4]. J.C. Jo, W.S. Kim, C.Y. Choi, Y.K. Lee, Numerical simulation of subcooled flow boiling heat transfer in helical tubes, ASME Journal of Pressure Vessel Technology 131, 2009.
[5]. J.S. Jayakumar, S.M. Mahajani, J.C. Mandal, K.N. Iyer, P.K. Vijayan, Thermal hydraulic characteristics of air-water two-phase flows in helical pipes, Chemical Engineering Research and Design 88, 501-512, 2010.
[6]. T.T. Chandratilleke, N. Nadim, R. Narayanaswamy, An investigation of flow boiling with secondary flow interaction in curved pipes, ECI 8th International Conference on Boiling and Condensation Heat Transfer, Lausanne, Switzerland, 3-7 June 2012.
[7]. R.C. Xin, A. Awwad, Z.F. Dong, M.A. Ebadian, H.M. Soliman, An investigation and comparative study of the pressure drop in air-water two-phase flow in vertical helicoidal pipes, International Journal of Heat and Mass Transfer 39 (4), 735-743, 1996.
[8]. L. Guo, Z. Feng, X. Chen, An experimental investigation of the frictional pressure drop of steam-water two-phase flow in helical coils, International Journal of Heat and Mass Transfer 44, 2601-2610, 2001.
[9]. L. Zhao, L. Guo, B. Bai, Y. Hou, X. Zhang, Convective boiling heat transfer and two-phase flow characteristics inside a small horizontal helically coiled tubing once-through steam generator, International Journal of Heat and Mass Transfer 46 (25), 4779-4788, 2003.
[10]. L. Santini, A. Cioncolini, C. Lombardi, M. Ricotti, Two-phase pressure drops in a helically coiled steam generator, International Journal of Heat and Mass Transfer 51, 4926-4939, 2008.
[11]. B.K. Akagawa, T. Sakaguchi, M. Ueda, Study on a gas-liquid two-phase flow in helically coiled tubes, Bulletin of the Japan Society of Mechanical Engineers 14(72), 564-571, 1971.
[12]. Y. Murai, H. Oiwa, T. Sasaki, K. Kondou, S. Yoshikawa, F. Yamamoto, Backlight imaging tomography for gas-liquid two-phase flow in a helically coiled tube, Measurement Science and Technology 16, 1459-1468, 2005.

NUMERICAL SIMULATION OF TURBULENT HEAT TRANSFER IN LIQUID METAL ALONG A HEATED ROD IN AN ANNULUS

S. HERBST, T. WETZEL
Institute for Nuclear and Energy Technologies, Karlsruhe Institute of Technology
Hermann-von-Helmholtz-Platz 1, D-76344 Eggenstein-Leopoldshafen – Germany

T. BAUMANN
Institute of Fluid Mechanics, Karlsruhe Institute of Technology
Kaiserstrasse 10, D-76131 Karlsruhe – Germany

ABSTRACT

Liquid metals are considered for an effective cooling in several nuclear applications. Particularly in this context, a safe design is indispensable and thus careful experimental as well as numerical investigations of the thermal hydraulic and heat transfer characteristics are required. Reliable Computational Fluid Dynamic (CFD) modelling is a challenge because of complex geometries, the anisotropy of turbulence and different turbulent length scales of the thermal and the momentum field due to low molecular Prandtl numbers of liquid metals. Dealing with high uncertainties at turbulence modelling, a validation including characteristic flow scenarios is necessary. In this context, a well-established eddy viscosity model in combination with a turbulent transport heat flux model (HFM) is applied to a pin simulator with lead bismuth eutectic (LBE) as coolant. Two transport equations are solved for the Reynolds stresses and five for the turbulent heat fluxes, the temperature variance and its dissipation. In this work a comparison of the CFD results is made with experimental data at thermal developing flow conditions at a Reynolds number $Re = 237000$. The numerical results exhibit good agreement with measured data of a heated rod experiment for the thermal field. The dimensions and parameters of the simulation and experiment have been chosen such that the model may now be used for dimensioning e.g. heat transfer experiments in liquid metal cooling loops such as that for fuel rod bundles in Accelerator-driven Systems (ADS).

1. Introduction

Heat exchangers with liquid metal cooling such as fuel rod bundles are of great interest for nuclear applications. However, the high complexity is a challenge for both simulations and experiments. Therefore a heated rod in an isothermal annulus serves as a first step in a multi-level simulation and validation process. Due to the complex geometry and the high Reynolds numbers, Reynolds-averaged Navier-Stokes methods are applied for the simulation of the turbulent flow.

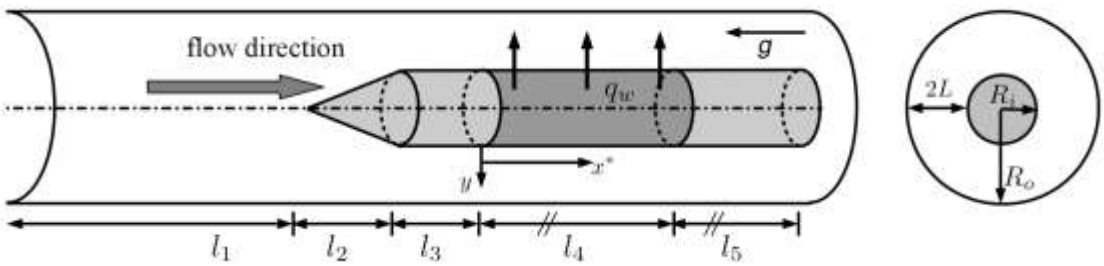

Fig 1. Geometry of heated rod simulation

The experimental setup, upon which the simulation is based, is located at Karlsruhe Liquid Metal Laboratory (KALLA). The simplified model is shown in Fig 1. For numerical studies, measurement equipment as well as spacers carrying the rod and the flow straightener upstream of the rod have been neglected. Regarding the setup and experimental results, detailed information may be taken from [1].
Concerning the applied inlet conditions, a fully developed isothermal pipe flow with a radius of $R_o = 0.03m$ is assumed. Also, isothermal boundary conditions are applied to the channel wall. The embedded rod is considered to be isothermal at its tip before a uniform heat flux is applied at the rod walls after one hydraulic diameter, which is defined by $D_h = 2(R_o - R_i) = 4L$. Along with the rod radius $R_i = 0.0041\ m$ the section length $l_2 = 0.0246\ m$ describes the shape of the cone. A second isothermal region with a length of $l_5 = 0.34\ m$ follows the heated section of $l_4 = 0.86\ m$. A dimensionless coordinate is set for the heated region by $x^* = \frac{x}{D_h}$.

2. Basic equations

The Reynolds averaged momentum and energy equations for incompressible flow under forced convection are expressed by

$$\frac{D\overline{u_\iota}}{Dt} = -\frac{1}{\rho}\frac{\partial \bar{p}}{\partial x_i} + \frac{\partial}{\partial x_j}\left(\nu\frac{\partial \overline{u_\iota}}{\partial x_j} - \overline{u'_\iota u'_\jmath}\right) \tag{1}$$

and

$$\frac{D\bar{T}}{Dt} = \frac{\partial}{\partial x_j}\left(\kappa\frac{\partial T}{\partial x_j} - \overline{u'_\jmath T'}\right), \tag{2}$$

with the kinematic viscosity ν, the density ρ and the heat conductivity κ. The Reynolds stresses $\overline{u'_\iota u'_\jmath}$ $(\forall\ i,j = 1..3)$ as well as the turbulent heat fluxes $\overline{u'_\jmath T'}$ need to be modelled with appropriate accuracy. Hence, an isotropic eddy viscosity model by Launder and Sharma (LS) [2] is applied for the momentum equations.

2.1. Heat flux modelling

Heat flux modelling is often based on an analogy of turbulent heat flux and turbulent momentum transport. While the turbulent viscosity ν_t is calculated by the LS model, the turbulent heat conductivity is determined according to equation (3) using a predefined turbulent Prandtl number Pr_t.

$$\kappa_t = \frac{\nu_t}{Pr_t} \tag{3}$$

The simplest way is an approach with a constant turbulent Prandtl number of $Pr_t = 0.9$, along with a gradient formulation for the turbulent heat fluxes:

$$\overline{u'_\iota T'} = -\kappa_t\frac{\partial \bar{T}}{\partial x_i}. \tag{4}$$

A more accurate approach for low molecular Prandtl numbers is given by Kays [3] who determines the turbulent Prandtl number by the expression:

$$Pr_{t,Kays} = 0.7\frac{\nu}{\nu_t Pr} + 0.85. \tag{5}$$

Besides using algebraic correlations, turbulent heat fluxes can also be calculated by solving transport equations. The second order heat flux model solves one equation for each heat flux $(\overline{u'_\iota T'}, \forall\ i = 1..3)$:

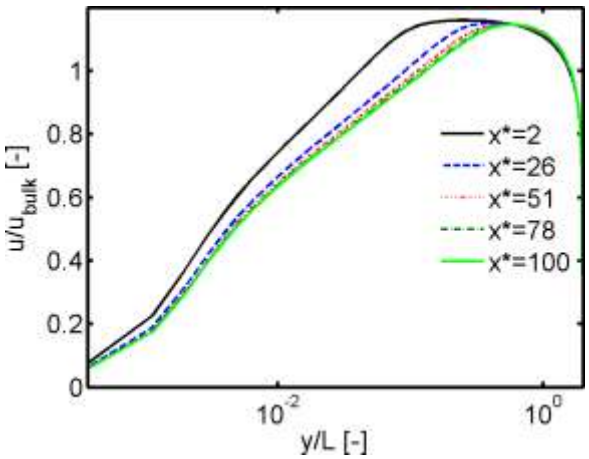

Fig 2. Velocity profiles at several axial positions for Re=237000

$$\frac{D\overline{u'T'}}{Dt} = -\left(\overline{u'_\iota u'_\jmath}\frac{\partial\overline{T'}}{\partial x_j} + \overline{u'_\jmath T'}\frac{\partial\overline{u_\iota'}}{\partial x_j}\right) - A + \phi + D_{u'T'} + \epsilon_{u'T'}, \tag{6}$$

with the buoyancy term A, the temperature-pressure-gradient correlation ϕ, the diffusion term $D_{u'T'}$ and the dissipation $\epsilon_{u'T'}$. Two additional equations are solved for the temperature variance and its dissipation $\epsilon_{T'T'}$.

$$\mathrm{u}_j\frac{\partial\overline{T'T'}}{\partial \mathrm{x}_j} = \overline{u'_\jmath T'}\frac{\partial\overline{T'}}{\partial x_j} + D_{T'T'} + \epsilon_{T'T'}\,, \tag{7}$$

with the diffusion $D_{T'T'}$ and the dissipation $\epsilon_{T'T}$. Baumann et al. [4] calibrated such a model to match the special characteristics of liquid metals. Detailed information about the modelling and the calibration might also be taken from [5].

3. Results and Discussion

Due to the high Reynolds number of $Re = 237000$ and the low heating of $\dot{q} = 1.35 \cdot 10^5\ W/m^2$

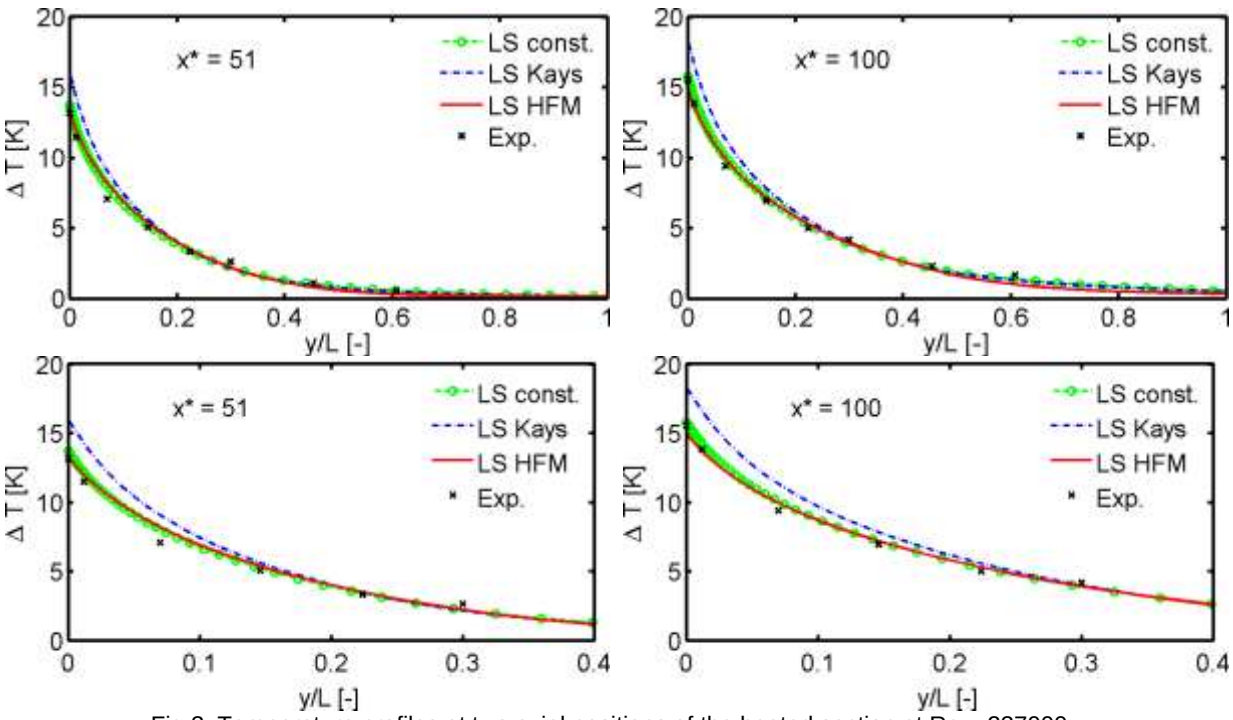

Fig 3. Temperature profiles at two axial positions of the heated section at Re = 237000

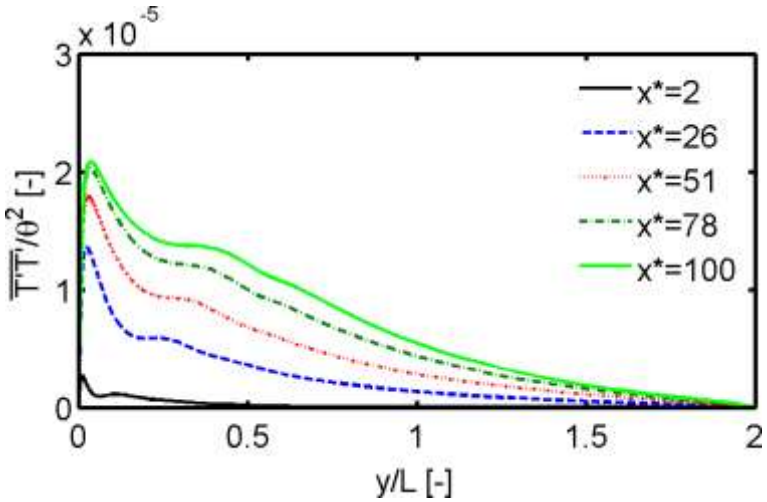

Fig 4. Temperature variance at several axial positions in the heated section for Re=237000 and Pr=0.025

buoyancy has no excessive impact on the flow field, which justifies that the process of heat transfer can be considered as pure forced convection [1].

Velocity profiles are given in Fig 2 at different axial positions x^*along the heated section. The maximum velocity decreases from $x^* = 0$ to higher x^* while its actual position in the gap moves to higher y/L values.

Fig 3 shows temperature profiles at two axial positions of the heated section. The displayed numerical results exhibit good agreement with the measured data, especially the more advanced heat flux model but also the supposed less accurate modelling of a constant turbulent Prandtl number. The Kays correlation seems to overestimate the turbulent Prandtl number, which then leads to a higher heating with a deviation of ΔT of 21% for $x^* = 51$ and 18% for $x^* = 100$, respectively.

The temperature variance, calculated by the heat flux model, is displayed in Fig 4, with $\theta = qL/\lambda$. It increases with x^* which can be explained by a higher production rate caused by an increased turbulent heat flux in wall normal direction, see equation 7. While in some distance from the wall $\overline{T'T'}$ still increases with higher x^* values, the total maximum is already reached at $x^* \approx 80$. The maximum is located close to the wall, which is caused by high temperature gradients at the heated surface and high turbulent heat fluxes which are displayed in Fig 5. At the rod surface the heat fluxes are equal to zero which follows from the no-slip condition. This has a direct impact on the temperature variance which also falls to zero at $x^* = 0$.

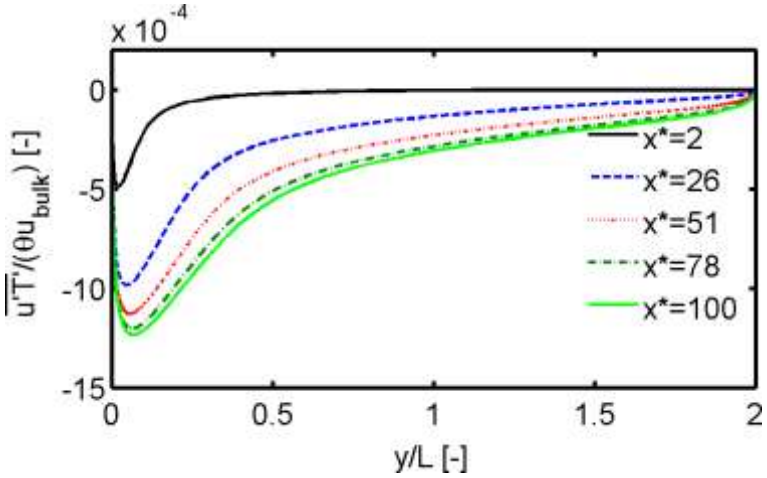

Fig 5. Turbulent heat flux in normal direction to the heated rod surface at Re=237000 and Pr=0.025

4. Conclusion

RANS simulations with different approaches for turbulent heat flux modelling have been applied to a heated rod for a high Reynolds number and a low Prandtl number (LBE) coolant. The results show good agreement with experimental data measured at KALLA. Thus a validation of the turbulence model is achieved in a complex geometric scenario at developing flow conditions.

A deviation of a suspected more accurate correlation for the turbulent Prandtl number is observed compared to the constant Pr_t modelling. As the LS model does not consider the anisotropy of the momentum field, it may lead to an insufficient prediction of ν_t, which then has a direct impact on the modelled eddy diffusivity. Anisotropic models, as for instance described in [5] and [6], will therefore be of interest for our further investigations.

In the presented combination the model can now be used for simulating heat exchangers with liquid metal cooling circuits. However, further validation is recommended for complex geometries.

5. References

[1] A. Loges, T. Baumann, L. Marocco, and T. Wetzel, "Experimental investigation on turbulent heat transfer in liquid metal along a heated rod in a vertical annulus," in *the 14th International Topical Meeting on Nuclear Reactor Thermal Hydraulics*, Toronto, 2011, pp. 25-29.

[2] B.E. Launder and B.I. Sharma, "Application of the energy-dissipation model of turbulence to the calculation of flow near a spinning disc," *Letters in heat and mass transfer*, vol. 1, pp. 131-138, 1974.

[3] W.M. Kays, "Turbulent Prandtl Number - Where Are We?," *Journal of Heat Transfer, Transactions ASME*, vol. 116, pp. 284-295, 1994.

[4] T. Baumann, H. Oertel jr., R. Stieglitz, and T. Wetzel, "Validation of RANS Models for Turbulent Low Prandtl Number Flows," in *the 9th International Meeting on Nuclear Thermal-Hydraulics*, Kaohsiung, 2012.

[5] T. Baumann, "Turbulenzmodellierung von Strömungen niedriger molekularer Prandtlzahl," 2012.

[6] A. Hellsten, "New two-equation turbulence model for aerodynamics application," Helsinki University of Technology, Dissertation 2004.

European Nuclear Society
Rue Belliard 65
1040 Brussels, Belgium
Telephone: +32 2 505 30 50 - FAX: +32 2 502 39 02
enc2012@euronuclear.org
www.enc-2012.org